atmosphere

MDPI

Article

Spatial Hotspots and Long-Term Changes in Rapid Temperature Flip Events Across China

Runkun Zhang [1,2], Xinyue Sun [1] and Miaoni Gao [1,*]

[1] School of Geographical Sciences, Nanjing University of Information Science and Technology, Nanjing 210044, China
[2] Changwang School of Honors, Nanjing University of Information Science and Technology, Nanjing 210044, China
* Correspondence: gaomn@nuist.edu.cn

Abstract

In recent decades, intensified temperature variability has increased the likelihood of abrupt transitions between anomalously cold and warm conditions, exerting substantial ecological and societal impacts. This study identifies rapid temperature flip events (RTFEs), including cold-to-warm transition events (C2Ws) and warm-to-cold transition events (W2Cs), across China using the CN05.1 gridded daily mean temperature data for 1961–2022, and further reveals their regional heterogeneity and long-term changes. Eastern China represents a hotspot of RTFEs, exhibiting higher frequencies and stronger intensities compared with western China. RTFEs are most frequent in spring, followed by summer. Over the period 1961–2022, both C2W and W2C became more frequent and more intense, with W2C showing a larger increase in frequency of 0.54 events century^{-1} and a larger increase in intensity of 0.29 s.d. century^{-1}, compared with increases of 0.01 events century^{-1} and 0.11 s.d. century^{-1}, respectively, for C2W. In addition, significant decadal changes in both types of events were observed across large areas of China during the 1990s–2000s and 2010s, following a high–low–high pattern. Analysis across the seven natural sub-regions reveals distinct high-hazard areas where RTFE hotspots coincide with increasing frequency and intensity: the eastern monsoonal regions of China for W2Cs and Inner Mongolia for both event types. These findings contribute to addressing climate change and mitigating the risk of RTFEs.

Keywords: China; decadal changes; hotspots; long-term trends; rapid temperature flip events

Check for updates

Academic Editor: Graziano Coppa

Received: 1 April 2026
Revised: 2 May 2026
Accepted: 12 May 2026
Published: 14 May 2026

Copyright: © 2026 by the authors. Licensee MDPI, Basel, Switzerland. This article is an open access article distributed under the terms and conditions of the Creative Commons Attribution (CC BY) license.

1. Introduction

The Sixth Assessment Report of the Intergovernmental Panel on Climate Change concludes that extreme events have become more frequent and intense across most land regions, which are projected to become more frequent with further global warming [1]. Numerous previous studies have focused on individual extreme events, such as cold waves or heatwaves [2,3]. In recent years, it has been increasingly recognized that compound extreme events often cause greater damage than isolated events [4,5]. Among them, 'temperature whiplash' has received growing attention and is characterized by abrupt transitions between anomalous cold and warm conditions [6]. It is also commonly referred to as a rapid temperature flip event (RTFE) and can be viewed as the temperature manifestation of 'weather whiplash' [7,8].

RTFEs cause rapid and intense temperature fluctuations that damage natural systems and human communities, because the time available for physiological and societal adaptation is very limited [6]. RTFEs can promote premature crop flowering in 'false spring' and increase vulnerability to subsequent anomalous cold spells, which disrupt growth rhythms and reduce yields in crops such as maize, winter wheat, and rice [9–11]. In addition, RTFEs occur abruptly and are difficult to predict, resulting in substantial societal impacts and serious risks to human health [12–14]. For example, in January 2026, a wave of low temperatures swept southern China, and Shanghai shifted from unusually warm conditions (about 20 °C, 68 °F) to rare snowfall within a week, leading to snow and icy road conditions that prompted road closures and disrupted transportation, while the persistent cold further interfered with residents' daily activities [15].

RTFEs have increasingly been identified using unified methods across different regions worldwide, and they are generally classified into two types: cold-to-warm and warm-to-cold abrupt reversals over relatively short timescales [7,16,17]. Regional studies have shown that RTFEs are closely linked to mid-latitude Rossby wave trains and atmospheric blocking, and that their occurrence is strongly modulated by variability in the westerly jet [16,18]. Recent global assessments have consistently quantified an intensification of rapid temperature change on short timescales under anthropogenic warming, using historical datasets and future projections to evaluate evolving risks and population exposure [17,19]. Across the global regions defined by the Intergovernmental Panel on Climate Change, over 60% have experienced more frequent, more intense, and faster RTFEs since 1961, and this tendency is projected to extend to most regions in the future [7].

China spans diverse climate regimes and is characterized by complex topography, resulting in pronounced regional climatic contrasts [20]. Moreover, it is frequently affected by both extratropical and tropical cyclones, which are often accompanied by rapid temperature variations on short timescales, underscoring the need to identify RTFEs and characterize their features across China [21,22]. Several studies have investigated the underlying causes of RTFEs in China in specific seasons or regions, whereas their patterns across China remain unclear. Consistent evidence indicates that the frequency of RTFEs in winter has increased in China, particularly for warm-to-cold transition [23,24]. Temperature whiplash occurring in winter over North China and in spring over eastern China are closely associated with the southeastward propagation of Eurasian wave-train anomalies [6,18]. At the annual scale, both cold-to-warm and warm-to-cold RTFEs were positively correlated with elevation and negatively correlated with latitude in the Sanjiang Plain, and their occurrence trends shifted from decreasing to increasing after 1980 [25].

Previous studies have advanced the understanding of RTFEs in China, yet significant gaps remain. Most existing studies have focused on single-type warm or cold extremes, or on limited regions, rather than on rapid transitions between the two at the national scale. In addition, inconsistencies in identification methods among studies have hindered direct comparisons across regions and between different types of RTFEs. Consequently, a systematic national-scale assessment of their spatial distribution, seasonal characteristics, and long-term changes is still lacking. To address these gaps, this study uses the CN05.1 gridded daily mean temperature data and a unified identification framework to systematically investigates RTFEs across China during 1961–2022, including both C2Ws and W2Cs. By providing a consistent comparison of the two event types at the national scale, this study addresses two key questions: (1) What are the spatial patterns and long-term changes in RTFE across China? and (2) How does RTFE hazard differ across different regions of China? The results provide a comprehensive climatological picture of RTFEs in China and a basis for understanding and mitigating their ecological and societal impacts.

2. Data and Methods

2.1. Study Area

The study area is mainland China (MC), covering over 9 million square kilometers (73–135° E, 18–53° N). The wide geographic extent and complex topography of MC lead to substantial spatial heterogeneity in regional climate conditions. Natural regionalization is commonly conducted according to regional environmental patterns. Based on multi-year mean temperature, precipitation, and moisture regimes, MC is divided into seven natural sub-regions [26,27]. These sub-regions and their standardized abbreviations are shown in Figure 1 and are defined as follows: (1) the temperate and warm-temperate desert of northwest China (DNW), (2) the temperate grassland of Inner Mongolia (GIM), (3) the temperate humid and sub-humid region of northeast China (TNE), (4) the warm-temperate humid and sub-humid region of north China (WTN), (5) the subtropical humid region of central and south China (SHC), (6) the Qinghai–Tibetan Plateau (QTP), and (7) the tropical humid region of south China (THS). The regional classification enables a deeper understanding of the spatiotemporal heterogeneity of RTFEs under distinct environmental settings. By comparing differences among the natural sub-regions, RTFE characteristics can be more comprehensively analyzed at both the national and sub-regional scales.

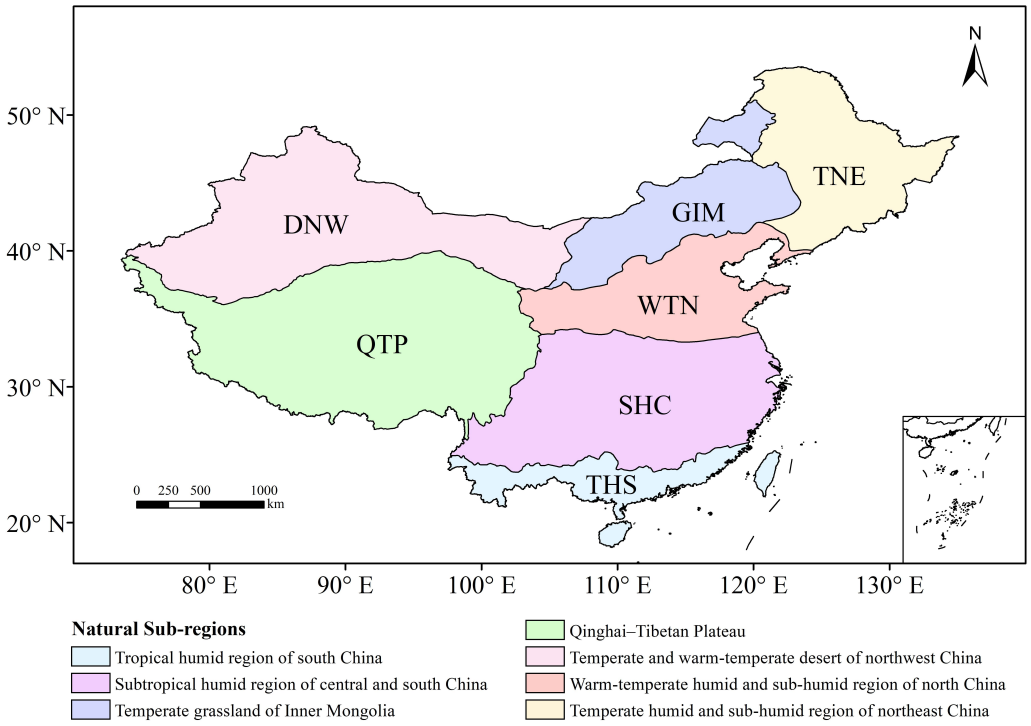


Figure 1. Spatial distribution of natural sub-regions in China.

2.2. Data

The daily mean temperature data used in this study are obtained from the CN05.1 gridded observational dataset, which has a horizontal resolution of 0.25° × 0.25° and covers the period 1961–2022. The Atlantic Multidecadal Oscillation (AMO) and the Pacific Decadal Oscillation (PDO), which are important low-frequency modes of decadal to multidecadal climate variability, are obtained from the Physical Sciences Laboratory of the National Oceanic and Atmospheric Administration for the period 1961–2022. The 200 hPa zonal wind data used in this study are derived from the National Centers for Environmental Prediction/National Center for Atmospheric Research reanalysis product, which provides monthly data with a horizontal resolution of 2.5° × 2.5° for the period 1961–2022.

2.3. Methods

2.3.1. Identification of RTFE

Several preprocessing procedures were applied to the CN05.1 gridded daily mean temperature data over China for 1961–2022 to identify RTFEs. RTFEs refer to abrupt transitions between anomalously cold and warm conditions within a short period, including cold-to-warm transition events (C2Ws) and warm-to-cold transition events (W2Cs), defined as an extreme cold (warm) event followed by an extreme warm (cold) event within a 5-day interval. Examples of C2W and W2C are shown in Figure 2. Following Wu et al. [7], extreme warm and cold events were defined using a threshold of ±1 standard deviation. The intensity of an RTFE was defined as the range of standardized temperature during the event, and the duration as the number of days from the end of the first extreme event to the onset of the subsequent extreme event.

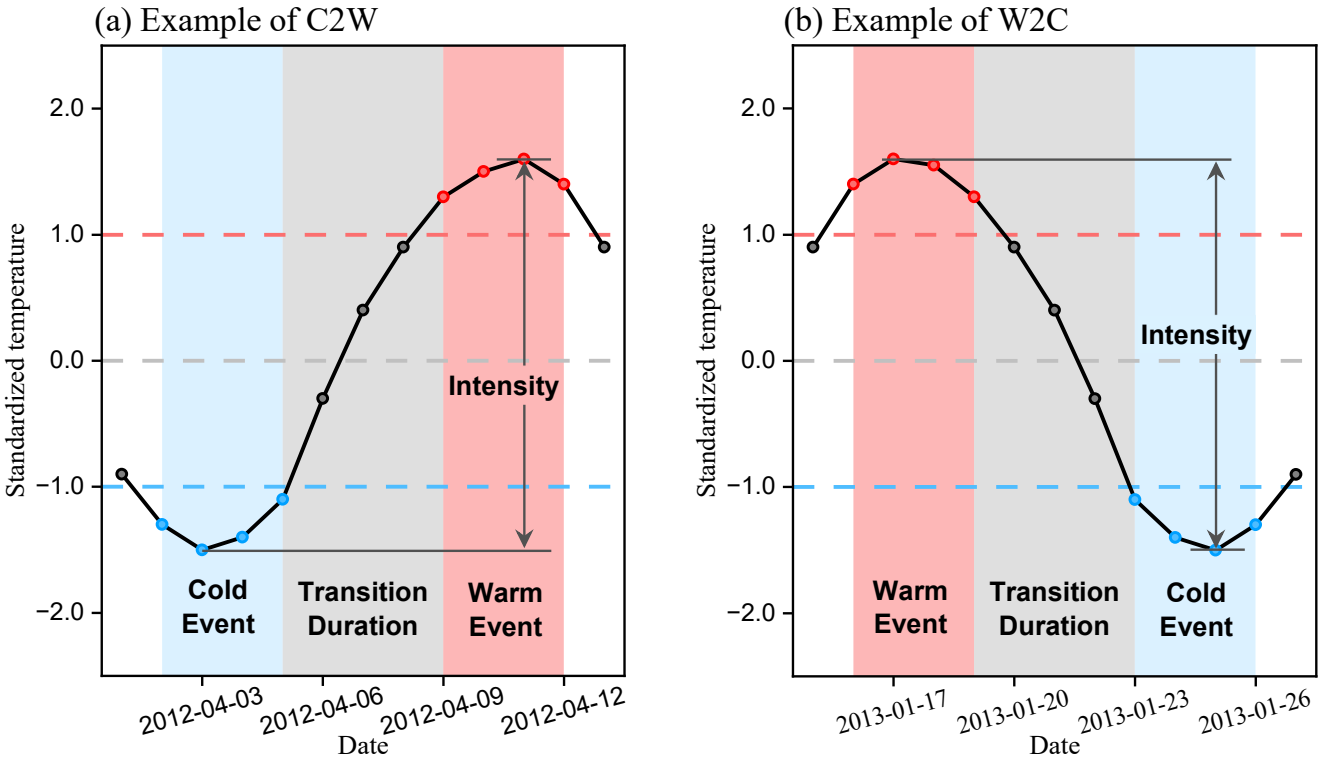


Figure 2. Examples of cold-to-warm (**a**) and warm-to-cold (**b**) transition events. Light blue, light gray, and light pink colors indicate the cold phase, transition phase, and warm phase of a RTFE, respectively.

Flowchart of RTFE identification is shown in Figure 3. Specifically, the daily mean temperature at each grid point was first detrended for each calendar day using a 31-day moving window centered on the target day. This window length was chosen as a compromise between retaining subseasonal temporal detail and obtaining a stable estimate of the background seasonal state. A third-degree polynomial was then fitted to the corresponding 62-year series to remove the seasonal cycle and long-term warming background before identifying RTFEs. Subsequently, the standardized anomaly series was smoothed with a 5-day moving average to reduce high-frequency day-to-day weather noise and to better highlight sustained temperature transitions relevant to RTFE identification. Smoothed detrended temperature data from 1961 to 1990 were used to calculate the multi-year standard deviation for each calendar day, representing climate variability largely independent of long-term trends. The standard deviation series was subsequently triplicated and concatenated so that a 31-day running window could be applied without edge effects. This procedure ensures that calendar days near the beginning and end of the year are

smoothed using a complete moving window and preserves continuity in the annual cycle of variability. After smoothing, only the central segment was retained for subsequent analysis. Finally, the smoothed detrended temperature data were standardized to identify extreme events. To assess the robustness of the identification method, sensitivity tests were performed for both the transition interval and the standard deviation threshold used to define extreme events. Alternative transition intervals of 3 and 7 days (Figures S1–S3) and standard deviation thresholds of 1.5 and 2.0 were tested (Figures S4 and S5). The results show that the main climatological and temporal characteristics of RTFEs remain qualitatively unchanged, indicating that the primary conclusions of this study are robust to these parameter choices.

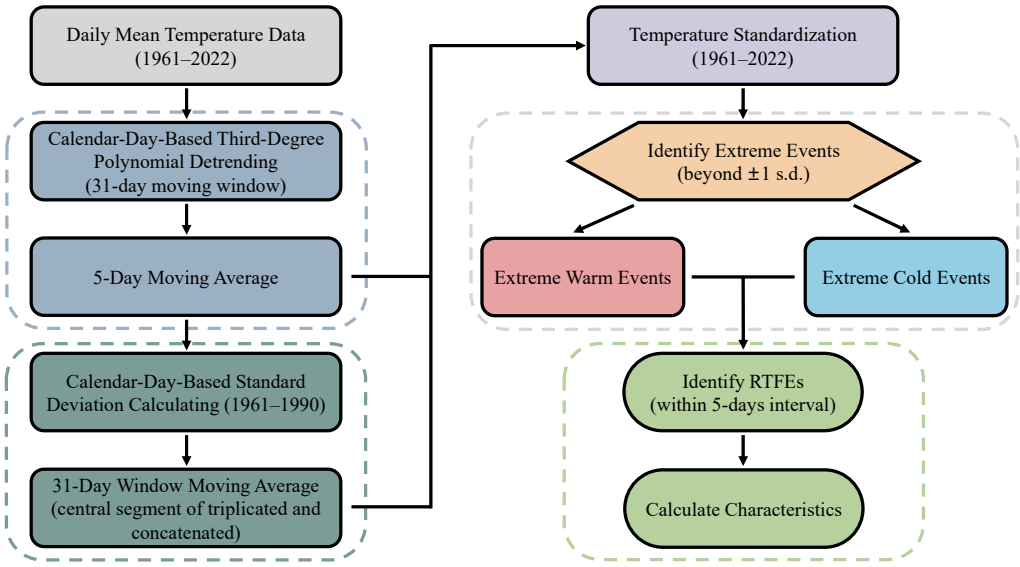


Figure 3. Flowchart of RTFE identification.

2.3.2. Statistical Methods

Seasons were defined following the conventional meteorological classification: winter (December–February, DJF), spring (March–May, MAM), summer (June–August, JJA), and autumn (September–November, SON). Long-term trends in the occurrence frequency, transition duration, and intensity of RTFEs at each grid point were estimated using ordinary least squares regression. Statistical significance was assessed using a modified non-parametric Mann–Kendall test, with p values < 0.05 considered statistically significant [28,29]. Regional trends for each natural sub-region of China were derived as area-weighted grid-point means [30]. Regional mean frequency was calculated as the area-weighted average of grid-point event frequencies. For event duration and intensity, regional means were computed using an area- and frequency-weighted averaging approach. The long-term ordinary least squares trends of spatially averaged occurrence frequency, duration, and intensity of RTFEs over MC remain similar when different ending years are applied, indicating that the reported trends are robust to endpoint effects (Figures S6 and S7).

Decadal changes in the RTFE frequency were identified using a moving two-sample t-test with multiple window lengths [31]. To further examine the relationships between RTFE frequency and modes of climate variability, Pearson correlation analysis was conducted between the regional frequency time series and the AMO and PDO indices [32]. The analysis was not conducted on the detrended temperature series itself, but on the frequency of RTFE occurrences. Therefore, the low-frequency climate signals related to AMO/PDO were not directly removed by the previous detrending procedure. Prior to the analysis, the

regional frequency time series were detrended using ordinary least squares regression and subsequently smoothed with a 5-year moving average, whereas the AMO and PDO indices were smoothed in the same manner.

3. Results

3.1. Spatial Patterns and Long-Term Changes in RTFEs Across China

To characterize the spatial patterns of RTFEs across MC, the climatological mean frequency, duration, and intensity of RTFE were analyzed over the period 1961–2022 (Figure 4). A clear west–east contrast emerges. Eastern China experiences RTFEs more frequently and with stronger intensities, whereas western China is generally characterized by fewer and weaker events. Superimposed on this large-scale pattern are several distinct hotspot regions where RTFEs occur particularly often. Using thresholds of more than 2.5 C2Ws per year and more than 3.4 W2Cs per year, prominent hotspot areas were identified on the Inner Mongolian Plateau and the Alxa Plateau, where both event types tend to occur with relatively short durations but strong intensities. Beyond these overlapping hotspots, C2W hotspots are also evident in the central Changbai Mountains and the Pearl River Delta, whereas W2C hotspots are more concentrated in southern China. In contrast, low RTFE frequencies are mainly found over major plateaus and basins. High-intensity centers show a different spatial signature, with exceptionally strong C2Ws appearing near Mount Everest, and strong W2Cs concentrated over the Hengduan Mountains.

Long-term trends in RTFEs reveal significant spatial heterogeneity across China, and notably, the hotspot regions identified from the climatological distribution are also the areas where both event types have increased most significantly over time (Figure 5). At the national scale, both C2Ws and W2Cs became more frequent and more intense during 1961–2022, indicating an overall strengthening of RTFEs across China. The increase is more pronounced for W2Cs, whose frequency trend (+0.54 events per century) is much larger than that of C2Ws (+0.01 events per century). In addition, C2Ws show a tendency toward longer duration, whereas W2Cs exhibit the opposite tendency. Overall, both event types have intensified, but the rise in national RTFE hazard is more strongly associated with W2C.

This long-term evolution is especially evident in the major hotspot regions, particularly on the Inner Mongolian Plateau and the Alxa Plateau, where both C2Ws and W2Cs show significant increases in frequency and intensity, together with shorter durations, with changes in W2Cs being more pronounced. Beyond these core regions, long-term changes display clear regional contrasts. In the Jianghuai region, C2Ws have decreased significantly and weakened in intensity, whereas in Northeastern China its duration has increased markedly, while W2Cs show the opposite tendency. Significant intensification of both event types is also evident in Northeastern China and in the southernmost and westernmost parts of the country.

3.2. Exploring RTFE Hazard Through Seasonal Variability and Regional Differences

To characterize the seasonal variations in RTFEs across China, the climatological mean characteristics of RTFEs were analyzed for each of the four seasons (Figure 6a–c). Both C2Ws and W2Cs exhibit clear seasonal cycles, with the highest occurrence in spring, when C2Ws reach 0.65 events per year and W2Cs reach 0.91 events per year, followed by summer. Seasonal contrasts are also evident in duration and intensity. C2Ws are shortest in winter, while W2Cs reach their minimum duration in spring. In terms of intensity, W2Cs show no obvious seasonal variation, whereas C2W intensity is markedly weaker in winter. Overall, W2Cs dominate across all seasons, exhibiting higher frequency and greater intensity than C2Ws.

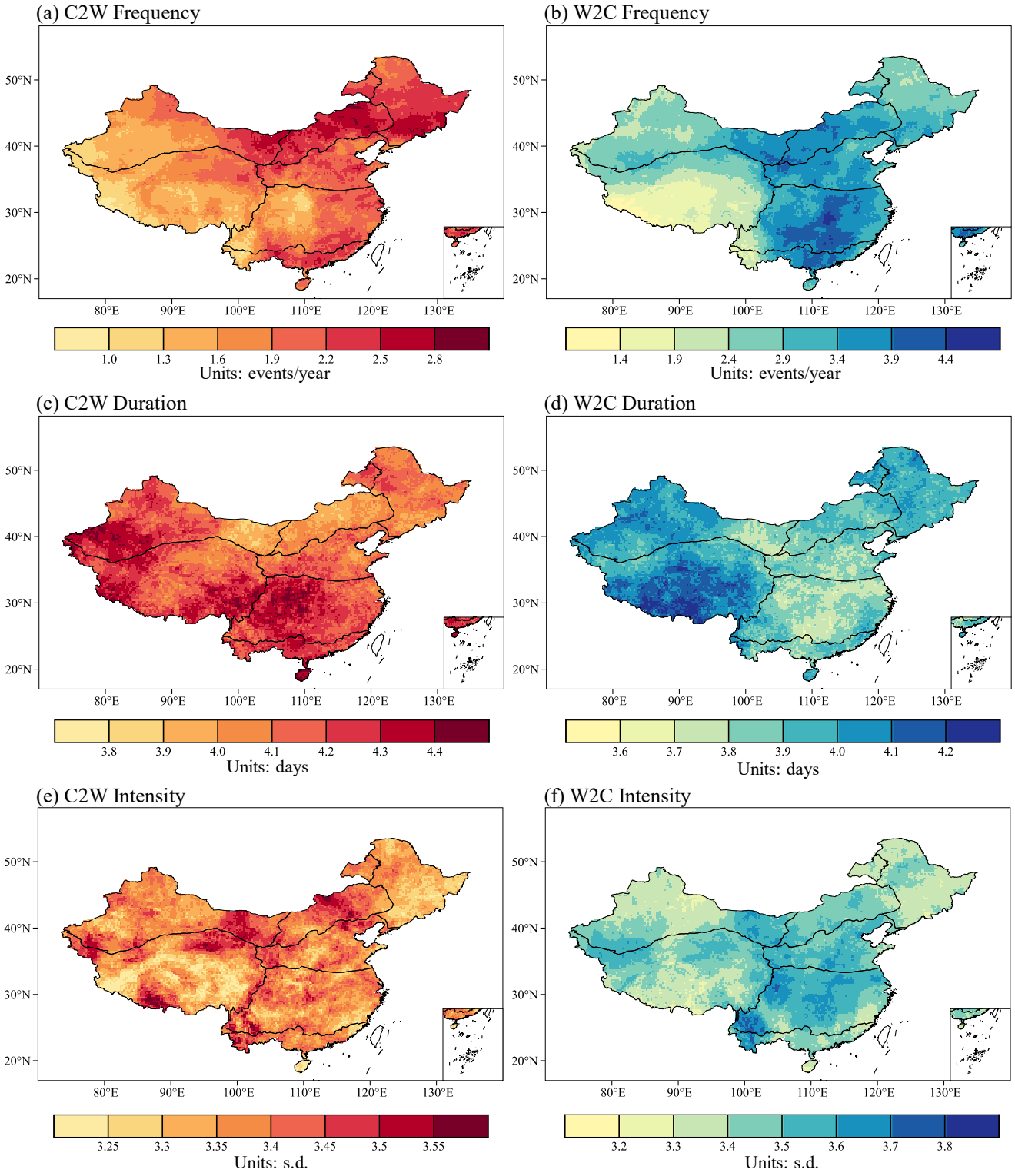


Figure 4. Spatial distributions of the climatological annual mean occurrence frequency (**a**,**b**), transition duration (**c**,**d**), and intensity (**e**,**f**) of the C2Ws (left panels) and W2Cs (right panels) across China over 1961–2022.

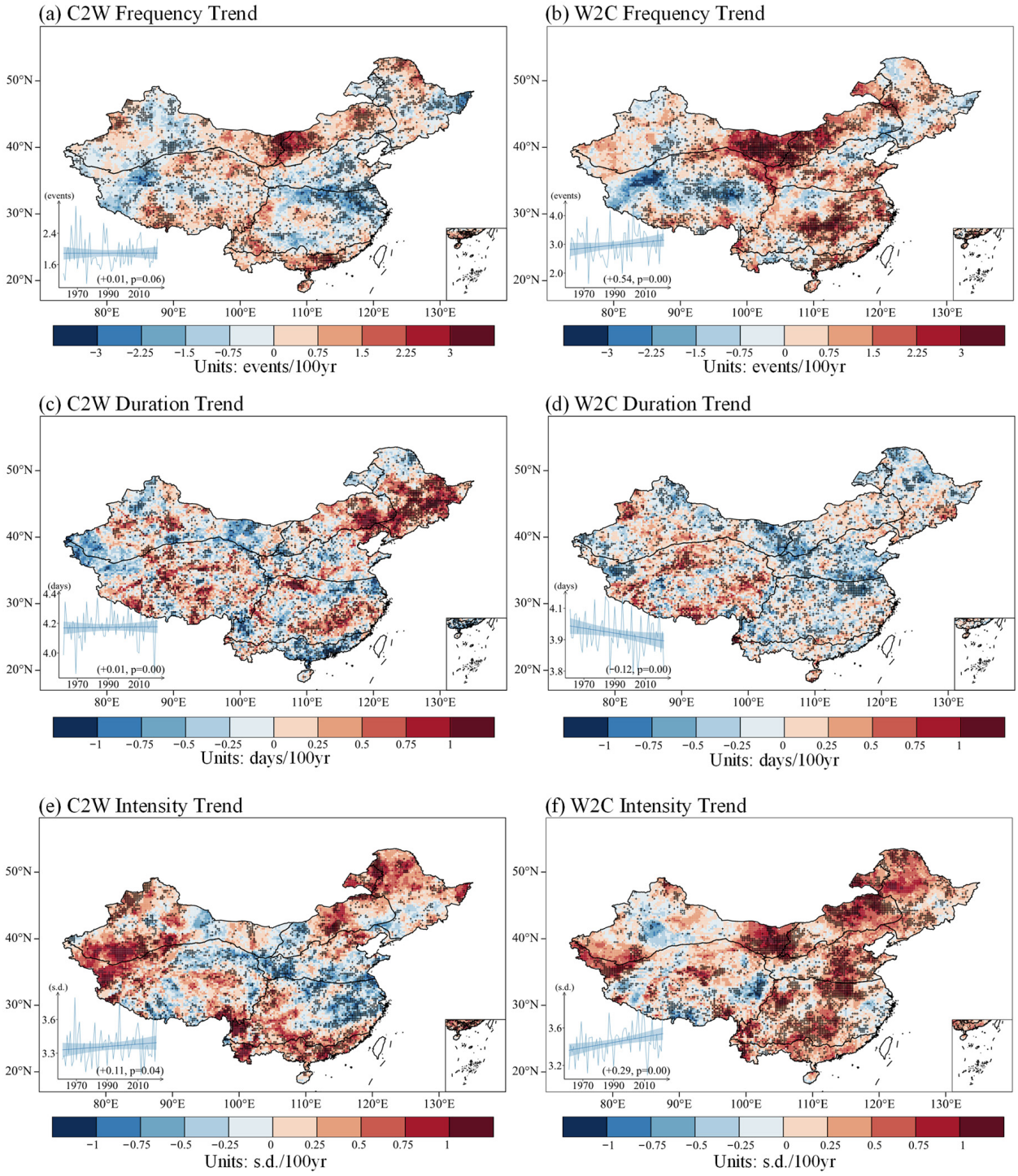


Figure 5. Spatial distributions of long-term trends in occurrence frequency (**a**,**b**), transition duration (**c**,**d**), and intensity (**e**,**f**) for C2Ws (left panels) and W2Cs (right panels) across China over 1961–2022. Plus signs (+) indicate significant trends. Insets show the corresponding time series of spatially averaged occurrence frequency, duration, and intensity over MC. Solid lines denote linear trends, shaded areas indicate the 90% confidence intervals, and values in parentheses give the trend slope per century and the corresponding *p* value.

Comparative analysis across seven natural sub-regions highlights pronounced spatial heterogeneity in RTFEs in China, reduces the influence of local-scale variability, and emphasizes regional-scale characteristics, facilitating the identification of high-hazard regions (Figure 6d–f). Across all seven natural sub-regions, both C2Ws and W2Cs occur most frequently in the temperate grassland of Inner Mongolia, the temperate humid and

sub-humid region of northeast China, and the warm-temperate humid and sub-humid region of north China. W2Cs generally occur more frequently than C2Ws and are associated with shorter durations and stronger intensities, indicating that W2Cs contribute disproportionately to regional RTFE hazard. C2Ws are most frequent in the temperate grassland of Inner Mongolia and the temperate humid and sub-humid region of northeast China, whereas C2Ws in the temperate grassland of Inner Mongolia showing short durations and strong intensities, whereas those in the temperate humid and sub-humid region of northeast China exhibit short durations but weak intensities. In contrast, W2Cs dominate the temperate grassland of Inner Mongolia, the subtropical humid region of central and south China, and the warm-temperate humid and sub-humid region of north China, exhibiting short durations and strong intensities, with slightly lower intensity in the temperate grassland of Inner Mongolia. Across all sub-regions, both event types are least frequent in the Qinghai–Tibetan Plateau, where they are characterized by long durations and strong intensities.

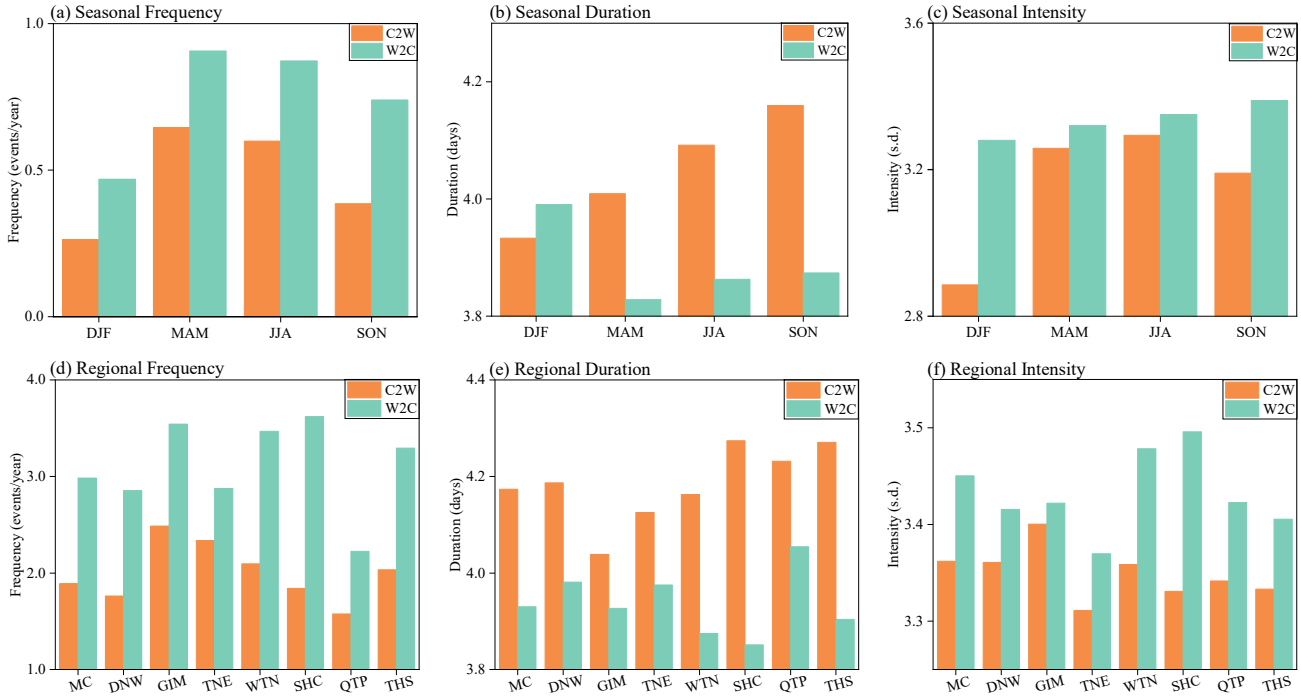


Figure 6. Seasonal and annual regional averages of C2Ws and W2Cs across China during 1961–2022. The upper panels present seasonal (DJF, MAM, JJA, SON) averages of occurrence frequency (**a**), transition duration (**b**), and intensity (**c**). The lower panels show annual averages for the entire mainland and for the seven natural sub-regions (**d**–**f**).

To assess whether the seasonal characteristics of RTFEs are consistent across regions, their regionally averaged characteristics were further examined across the seven natural sub-regions (Figure 7). Additionally, long-term trend analysis reveals distinct patterns for the two event types (Figure 8). High-hazard areas are characterized by RTFE hotspots that coincide with faster increases in both frequency and intensity during the peak season relative to other regions. The temperate grassland of Inner Mongolia emerges as the most active region, with both C2Ws and W2Cs exhibiting high frequency, short duration, and strong intensity in all seasons except winter. In spring, C2Ws reach their peak frequency, while W2Cs show the shortest duration, with both event types exhibiting significant increases in frequency and intensity. The subtropical humid region of central and south China and the warm-temperate humid and sub-humid region of north China represent

secondary high-hazard regions, where W2Cs are more dominant than in the temperate grassland of Inner Mongolia.

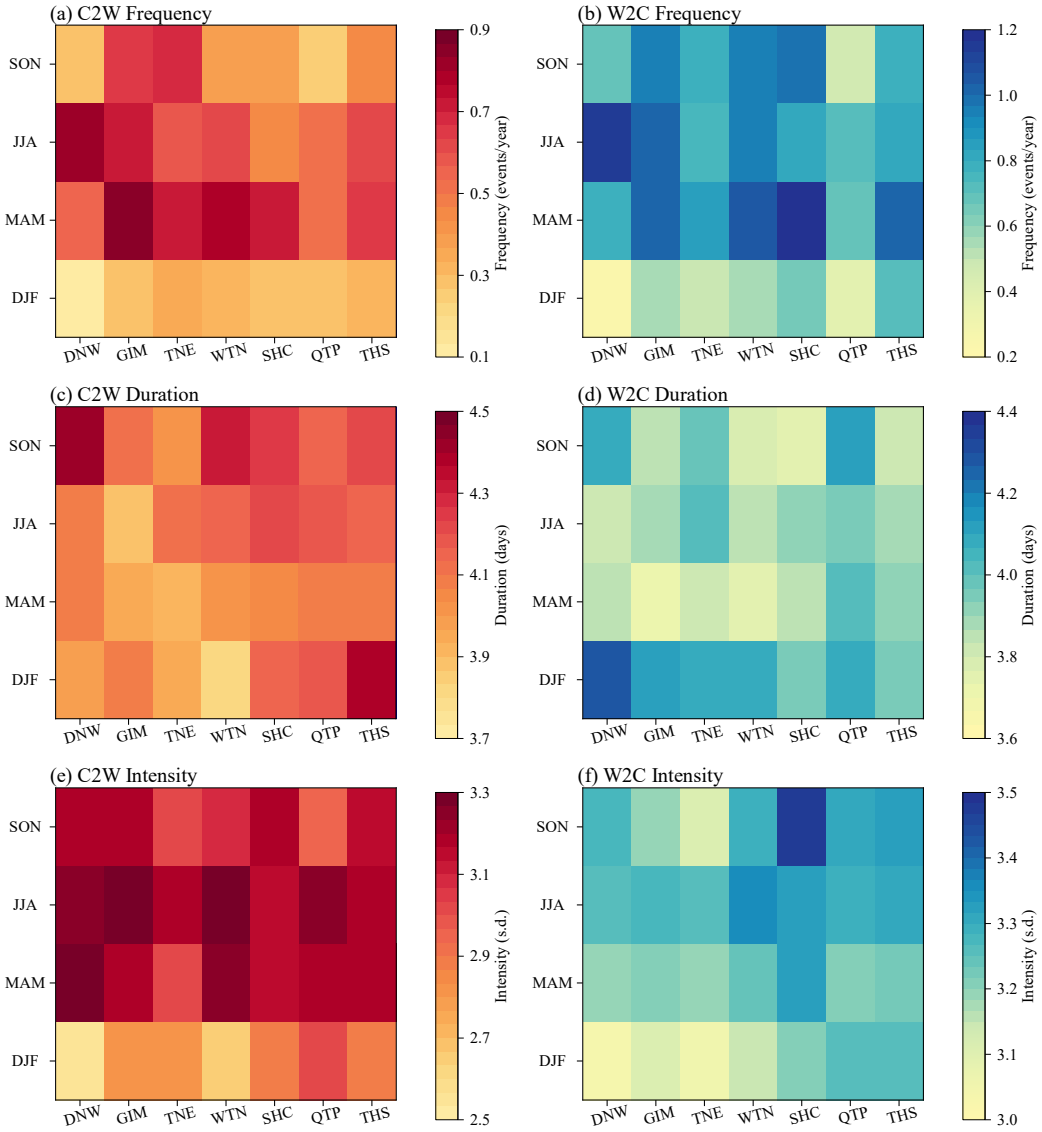


Figure 7. Regional averages of the climatological seasonal (DJF, MAM, JJA, SON) mean occurrence frequency (**a**,**b**), transition duration (**c**,**d**), and intensity (**e**,**f**) of the C2Ws (left panels) and W2Cs (right panels) across China over 1961–2022.

Across most regions, both types of events exhibit increasing frequency and strengthening intensity during the high-occurrence seasons of spring to autumn. In winter, when C2Ws are relatively infrequent, their intensity nonetheless increases in most regions. Overall, both types of events exhibit a general intensification in strength throughout the year. W2Cs show stronger consistency in increasing frequency and shortening duration across sub-regions, whereas C2Ws show stronger regional differentiation and offsetting trends, yielding a weak overall national signal. The frequency of C2W significantly increases or decreases only in a few regions, whereas W2Cs increase significantly across most sub-regions.

Seasonal changes are most pronounced during the transitional seasons of spring and autumn, with both event types exhibiting significantly enhanced intensity in the tropical humid region of south China. Spring, as the most active season for both event types, shows a consistent increase in frequency, accompanied by a shortening of duration and an intensification of strength. However, C2Ws exhibit a localized extension of duration

in a few regions. Autumn shows widespread shortening of duration, with events in this season being brief but intense. Winter generally displays smaller changes in frequency, although C2Ws have intensified in most regions, notably in the Qinghai–Tibetan Plateau, whereas W2C intensity shows slight weakening. In addition to the high-hazard areas, certain regions exhibit prominent high RTFE frequencies during specific seasons, including summer for both event types over the temperate and warm-temperate desert of northwest China, autumn for C2Ws across the temperate humid and sub-humid region of northeast China, and winter for W2Cs within the tropical humid region of south China.

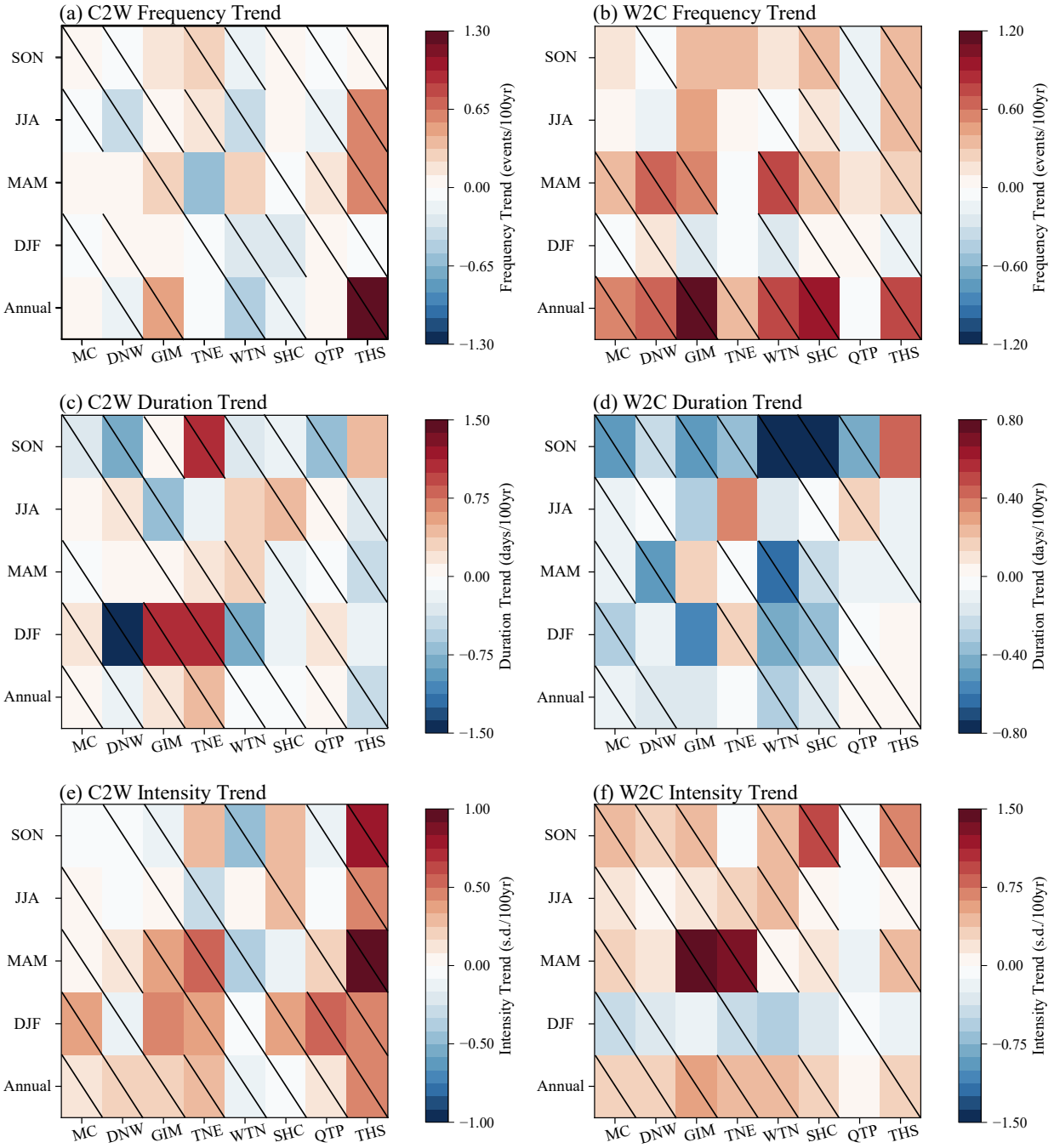


Figure 8. Long-term trends in regional averages of annual and seasonal (DJF, MAM, JJA, SON) occurrence frequency (**a**,**b**), transition duration (**c**,**d**), and intensity (**e**,**f**) for C2Ws (left panels) and W2Cs (right panels) across China over 1961–2022. Backslash signs (\) indicate significant trends.

3.3. Decadal Changes in RTFE Frequency

To detect decadal changes in RTFE frequency, a moving *t*-test was employed to identify significant shifts across the study period of 1961–2022. The results indicates that the frequency of the two event types in MC follows a high–low–high pattern, with the initial high phase further divided into relatively low and relatively high periods (Figures 9 and S8). The decadal changes in C2Ws generally lag behind those of W2Cs by several years. Specifically, a mild shift occurred in the 1970s, with W2Cs changing in 1972 and C2Ws in 1974, both marked by a moderate increase in frequency. A more significant shift was observed in the following decades of 1990s–2000s, with W2Cs declining between 1995 and 2002 and C2Ws between 2000 and 2005, both exhibiting a notable decrease in frequency. Subsequently, a marked increase in frequency occurred in 2010 for W2Cs and in 2012 for C2Ws.

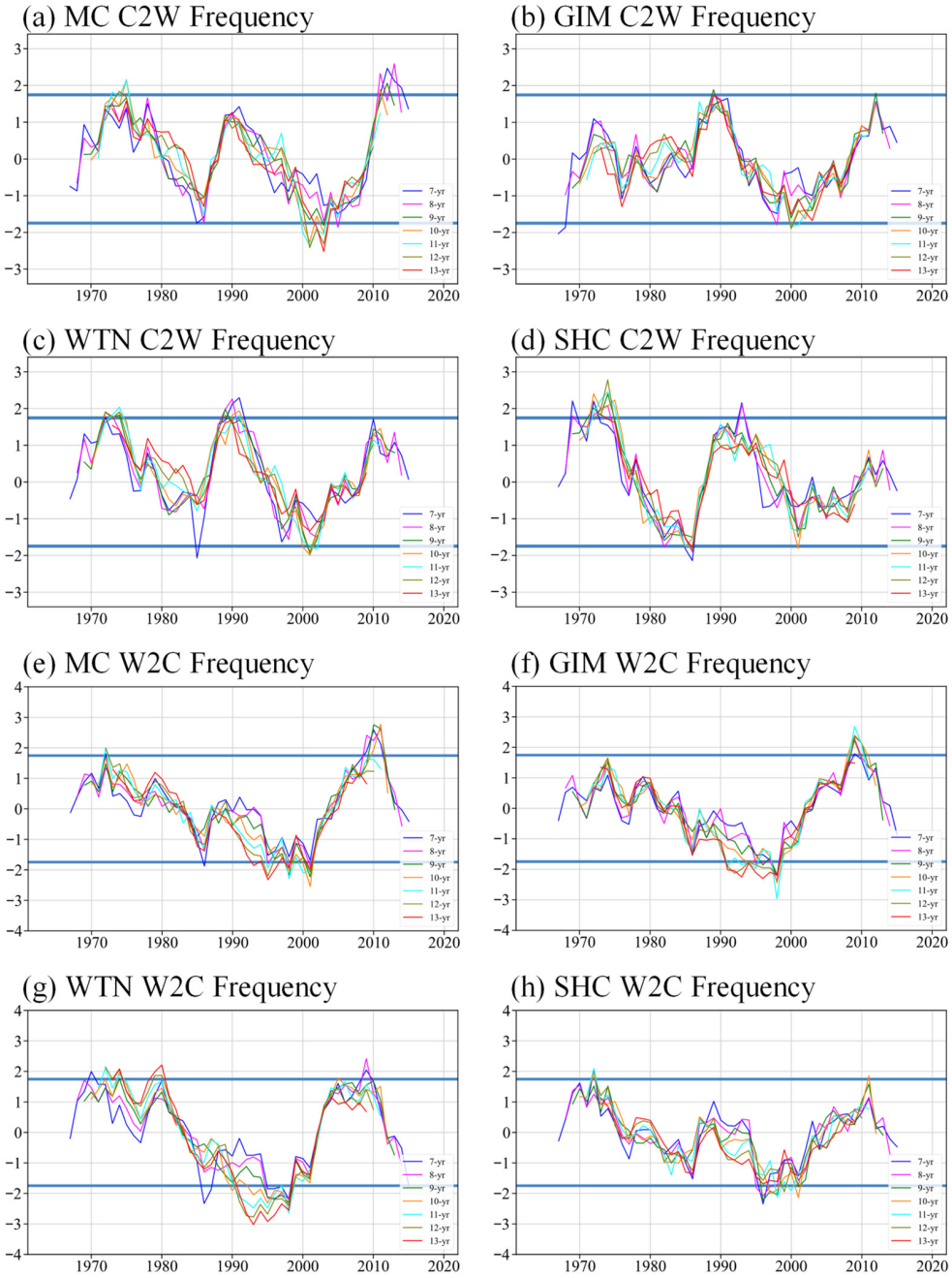


Figure 9. The moving *t*-test values of C2W (**a**–**d**) and W2C (**e**–**h**) frequencies during 1961–2022 using window lengths of 7–13 years over MC, GIM, WTN and SHC. The solid blue horizontal lines represent the 0.05 significance upper and lower bounds.

Decadal changes in high-hazard areas are largely consistent with those in MC, while certain sub-regions exhibit notable deviations from the national average. The temperate and warm-temperate desert region of northwest China displays the most distinct decadal changes, C2Ws show significant increases in 1979 and 2010, while W2Cs show notable rises in 1983 and 2010, with a significant drop in 1995. In the tropical humid region of south China, C2Ws experience a decline in 1986, transitioning from high to low frequency, while W2Cs decrease in 1986 and increases again in 2006. In Qinghai–Tibetan Plateau, W2Cs rise in 1991 and drops in 2001, following a low–high–low pattern, while C2Ws experience a decline in 1986. The temperate humid and sub-humid region of northeast China exhibits the smallest frequency fluctuations and lacks a clear decadal signal for either event type.

4. Discussion

Our findings can be further understood in relation to previous studies on climate variability and temperature extremes in China. Existing studies have shown that, under a warming climate, changes in mean temperature are often accompanied by shifts in temperature variability and in the occurrence of compound or transition-type extremes [33,34]. Previous work in China has also indicated that rapid temperature reversals are particularly active in eastern monsoonal regions and during the transitional seasons, where interactions between high-latitude cold air and low-latitude warm air are frequent and subseasonal variability is strong [35,36]. The spatial and seasonal features identified in this study are broadly consistent with these earlier findings, especially the greater activity of RTFEs in eastern China and the prominence of spring as the most active season.

At the same time, our results extend the existing literature in several respects. Most previous studies in China have focused on individual regions or on one type of rapid temperature transition, which has limited direct comparison across regions and between event types [37]. By applying a unified identification framework to the whole of China, this study provides a consistent comparison of both C2W and W2C events at the national scale. This allows us to identify not only their contrasting spatial patterns, but also their distinct long-term changes and high-hazard regions. In this sense, the present study complements earlier regional analyses and provides a broader climatological perspective on rapid temperature flip events in China.

To better interpret these findings, several possible contributing factors are discussed. The higher occurrence of RTFEs in eastern China may be attributed to both dynamic and thermodynamic factors. Eastern China lies in a transitional zone strongly influenced by the East Asian monsoon, where cold air outbreaks from higher latitudes frequently interact with warm and moist air masses from lower latitudes and adjacent oceans. This alternating influence of cold and warm air masses favors rapid temperature reversals on short timescales [38]. In addition, eastern China is a region of pronounced intraseasonal temperature variability, associated with active synoptic-scale disturbances and transient eddy activity over Eurasia, which further enhances the likelihood of abrupt temperature flips [35]. From a statistical perspective, the detrended calendar-day mean threshold corresponding to 1 s.d. is relatively lower in eastern China (Figure S9), implying that temperature anomalies can more readily exceed the local threshold under strong natural variability, thereby increasing the probability of identified RTFEs in this region (Figure S10). Further investigation is required to understand these factors from the perspectives of large-scale circulation and temperature diagnostics.

Beyond the spatial distribution discussed above, the long-term changes in RTFEs are further examined. The pronounced long-term changes in RTFEs identified in this study point to the influence of large-scale circulation and climate variability. Therefore, a brief discussion of some possible factors underlying these changes is attempted. RTFE

occurrence is often associated with cyclone activity, and the path, intensity, and frequency of cyclones are influenced by the position and strength of the subtropical jet [39]. This motivates further examination of whether the westerly jet has undergone notable changes during the study period, and whether such changes may be linked to the observed long-term evolution of RTFEs (Figure 10). The results indicated a significant strengthening trend of the mid-latitude subtropical jet over China during 1961–2022. It is primarily linked to changes in the meridional temperature gradient through thermal wind balance, with enhanced baroclinicity and variations in sea surface temperature gradients further reinforcing the jet [40,41]. The intensification of the subtropical jet may have enhanced cyclonic activity and increased RTFEs over China.

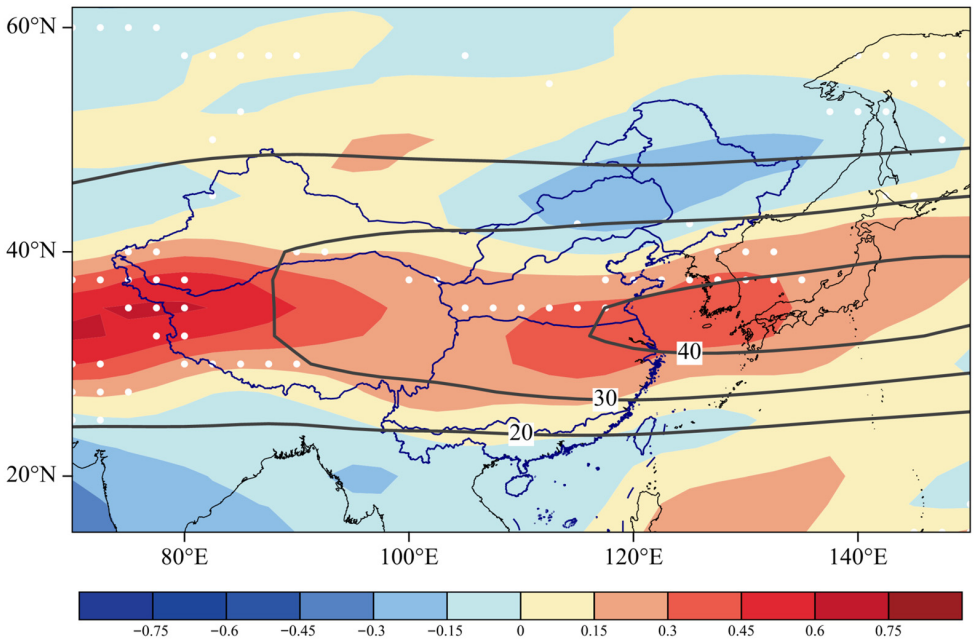


Figure 10. Annual climatological mean (unit: m s^{-1}) and trend (unit: m s^{-1} $decade^{-1}$) of zonal wind at 200 hPa. Gray contours showing the 1961–1990 climatological mean and shading indicating the 1961–2022 trend. Areas exceeding a significance level of 0.1 are indicated by white dots.

In addition, the observed long-term increases in RTFE frequency and intensity may also be linked to changes in regional temperature variability. Rapid temperature flips are more likely when cold air outbreaks from higher latitudes alternate more frequently with warm air advection from lower latitudes and adjacent oceans, a situation that is particularly common in eastern China under the influence of the East Asian monsoon [42]. In addition, enhanced intraseasonal temperature oscillations and active synoptic disturbances can amplify short-term temperature anomalies, increasing the likelihood that temperatures cross the thresholds used to identify RTFEs [43]. These factors may together contribute to the stronger trends observed in eastern China and other high-hazard regions. The larger increase in W2C may further reflect the combined effect of a warmer background climate and episodic cold-air intrusions, which favor abrupt reversals from warm to cold conditions. The specific impacts of these factors on RTFEs remain unclear and warrant further investigation.

Beyond the long-term trends discussed above, RTFEs also exhibit pronounced decadal variability. Such variability may be associated with large-scale modes of climate variability. The AMO and PDO are two major signals of interdecadal climate variability and may influence temperature variations over China through their effects on large-scale circulation [44,45]. Therefore, the correlations of RTFEs with the AMO and PDO were further analyzed to explore whether these modes may help explain the observed decadal changes in RTFEs (Figures 11 and S11). W2C frequency is positively correlated with the

AMO over non-plateau mid- and low-latitude China, with increases in the 1990s corresponding to its phase shift, whereas both C2Ws and W2Cs are negatively correlated with the PDO in mid-latitude regions, with changes around 1976 and 1997 opposing with its phase transitions. Specifically, the most significant PDO correlations with C2W frequency occur in the temperate and warm-temperate desert region of northwest China, with W2Cs in the temperate grassland of Inner Mongolia, and with both types in the warm-temperate humid and sub-humid region of north China. The AMO and PDO may influence RTFEs by modulating large-scale atmospheric circulation in response to sea surface temperature anomalies, while the specific pathways warrant further investigation [45,46]. However, the remaining regions that exhibit decadal variability but show no significant association with the AMO or PDO require further investigation to clarify the underlying mechanisms.

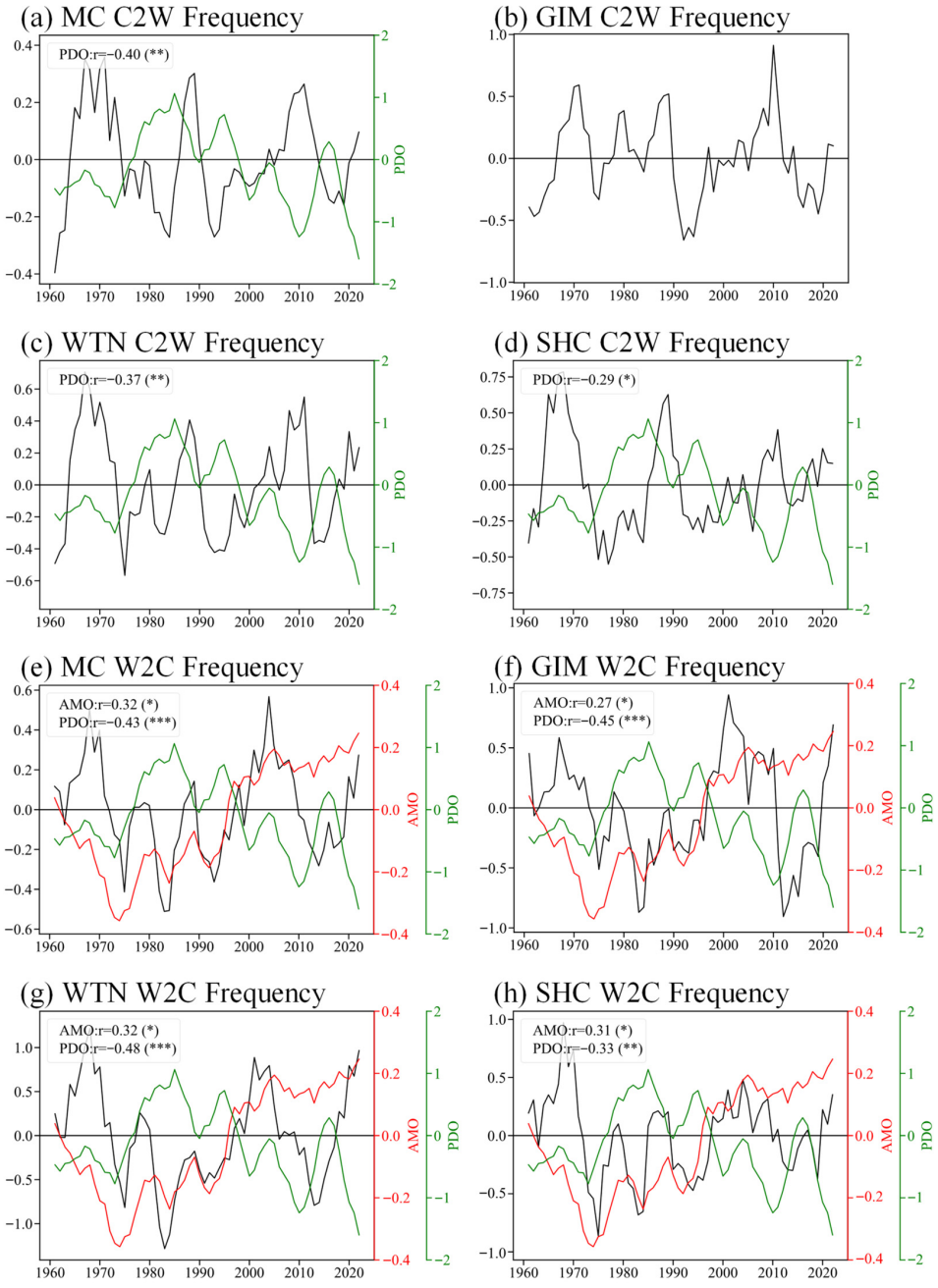


Figure 11. Pearson correlation analysis of C2W (**a**–**d**) and W2C (**e**–**h**) frequency time series with the AMO and PDO time series during 1961–2022 over MC, GIM, WTN and SHC. Significance levels are denoted by asterisks: * indicates a significant trend with p value < 0.05, ** indicates a significant trend with p value < 0.01, and *** indicates a significant trend with p value < 0.001.

Overall, the findings revealed the spatial distribution and temporal variability of RTFEs, providing a scientific basis for improving climate adaptation strategies tailored to region-specific sensitivities and seasonal vulnerabilities. However, the characteristics of RTFEs may vary depending on the identification criteria applied, while the underlying dynamical mechanisms remain insufficiently explored. In addition, the potential impacts of these events, as well as their future changes and associated risks under climate change, require further investigation to better support climate adaptation and disaster risk reduction efforts.

5. Conclusions

This study examines the spatial hotspots and long-term changes in RTFEs across China during 1961–2022. The results reveal a pronounced West–East contrast in RTFEs: eastern China experiences higher frequencies, shorter durations, and stronger intensities, while low-frequency areas in western China, mainly distributed over plateaus and basins, exhibit longer durations and weaker intensities. RTFEs also exhibit distinct seasonal cycles, with frequencies peaking in spring and relatively high in summer, and showing the most pronounced seasonal changes in spring and autumn. Over the period 1961–2022, both C2Ws and W2Cs became more frequent and more intense. W2Cs show a more pronounced frequency increase and a stronger association with national RTFE hazard. The frequencies of both event types show significant decadal variability across large areas of China during the 1990s–2000s and 2010s, characterized by a clear high–low–high pattern, with the initial high phase further subdivided into relatively low and high periods. High-hazard areas, where RTFE hotspots coincide with increasing frequency and intensity, are most pronounced in Inner Mongolia for both events, characterized by high frequency, short duration, and strong intensity across all seasons except winter, followed by the eastern monsoonal regions of China for W2Cs. These findings provide new insight into the climatological characteristics and long-term evolution of rapid temperature transitions, and may contribute to improving the assessment of associated ecological and societal hazards under a changing climate.

Supplementary Materials: The following supporting information can be downloaded at: https://www.mdpi.com/article/10.3390/atmos17050500/s1, Figure S1: Spatial distributions of the climatological annual mean occurrence frequency (a,b), transition duration (c,d), and intensity (e,f) of the C2Ws and W2Cs within three days; Figure S2: Spatial distributions of the climatological annual mean occurrence frequency (a,b), transition duration (c,d), and intensity (e,f) of the C2Ws and W2Cs within seven days; Figure S3: Seasonal averages of occurrence frequency (a,d), transition duration (b,e), and intensity (c,f) for RTFEs within three and seven days; Figure S4: The corresponding time series of spatially averaged occurrence frequency (a,d), transition duration (b,e), and intensity (c,f) of C2Ws and W2Cs identified using a 1.5 s.d. threshold over MC; Figure S5: The corresponding time series of spatially averaged occurrence frequency (a,d), transition duration (b,e), and intensity (c,f) of C2Ws and W2Cs identified using a 2.0 s.d. threshold over MC; Figure S6: The corresponding time series of spatially averaged occurrence frequency (a–d), transition duration (e–h), and intensity (i–l) for C2Ws over MC for the periods 1961–2010, 1961–2014, 1961–2018, and 1961–2022; Figure S7: The corresponding time series of spatially averaged occurrence frequency (a–d), transition duration (e–h), and intensity (i–l) for W2Cs over MC for the periods 1961–2010, 1961–2014, 1961–2018, and 1961–2022; Figure S8: The moving t-test values of C2W (a–d) and W2C (e–h) frequencies during 1961–2022 using window lengths of 7–13 years over DNW, TNE, QTP and THS; Figure S9: Spatial distributions of mean temperature corresponding to the calendar-day standard deviation threshold of 1 s.d over 1961–1990; Figure S10: Spatial distributions of the climatological annual mean occurrence frequency of the extreme warm events (a) and extreme cold events (b) across China over 1961–2022; Figure S11; Pearson correlation analysis of C2W (a–d) and W2C (e–h) frequency time series with the AMO and PDO time series during 1961–2022 over DNW, TNE, QTP and THS.

Author Contributions: R.Z.: Writing—original draft, Software, Methodology. X.S.: Writing—review and editing, Data curation. M.G.: Writing—review and editing, Validation, Conceptualization. All authors have read and agreed to the published version of the manuscript.

Funding: This research was funded by NUIST Students' Innovation Training Program.

Institutional Review Board Statement: Not applicable.

Informed Consent Statement: Not applicable.

Data Availability Statement: The CN05.1 dataset is derived from the Nansen-Zhu International Research Centre, Institute of Atmospheric Physics, Chinese Academy of Sciences at https://nzc.iap.ac.cn/content?aid=999&cid=24 (accessed on 12 December 2025) and is available upon reasonable request. The AMO and PDO indices and the 200 hPa zonal wind data used in this study are available from the Physical Sciences Laboratory of the National Oceanic and Atmospheric Administration at https://psl.noaa.gov/data/timeseries/AMO/ (accessed on 4 July 2025), https://psl.noaa.gov/pdo/ (accessed on 4 July 2025), and https://psl.noaa.gov/data/gridded/data.ncep.reanalysis.html (accessed on 6 July 2025). The analysis code is available on request from the authors.

Conflicts of Interest: The authors declare no conflicts of interest.

References

1. IPCC. Climate Change 2023: Synthesis Report. In *Contribution of Working Groups I, II and III to the Sixth Assessment Report of the Intergovernmental Panel on Climate Change*; Lee, H., Romero, J., Eds.; IPCC: Geneva, Switzerland, 2023; pp. 35–115. [CrossRef]
2. Chen, J.; Yang, J.; Zhou, M.; Yin, P.; Wang, B.; Liu, J.; Chen, Z.; Song, X.; Ou, C.-Q.; Liu, Q. Cold Spell and Mortality in 31 Chinese Capital Cities: Definitions, Vulnerability and Implications. *Environ. Int.* **2019**, *128*, 271–278. [CrossRef]
3. Anderson, G.B.; Bell, M.L. Heat Waves in the United States: Mortality Risk during Heat Waves and Effect Modification by Heat Wave Characteristics in 43 U.S. Communities. *Environ. Health Perspect.* **2011**, *119*, 210–218. [CrossRef]
4. Sun, P.; Bian, Y.; Yu, S.; Yao, R.; Wang, Z.; Zhang, Q.; Chen, W.; Ge, C.; Ma, Z.; Du, W. Are Longer and More Intense Heatwaves More Prone to Extreme Precipitation? *Glob. Planet. Change* **2024**, *236*, 104428. [CrossRef]
5. Zscheischler, J.; Martius, O.; Westra, S.; Bevacqua, E.; Raymond, C.; Horton, R.M.; Van den Hurk, B.; AghaKouchak, A.; Jézéquel, A.; Mahecha, M.D.; et al. A Typology of Compound Weather and Climate Events. *Nat. Rev. Earth Environ.* **2020**, *1*, 333–347. [CrossRef]
6. Ma, S.; Zhu, C. Atmospheric Circulation Regime Causing Winter Temperature Whiplash Events in North China. *Int. J. Climatol.* **2021**, *41*, 917–933. [CrossRef]
7. Wu, S.; Luo, M.; Lau, G.N.-C.; Zhang, W.; Wang, L.; Liu, Z.; Lin, L.; Wang, Y.; Ge, E.; Li, J.; et al. Rapid Flips Between Warm and Cold Extremes in a Warming World. *Nat. Commun.* **2025**, *16*, 3543. [CrossRef] [PubMed]
8. Lee, C.C. Weather Whiplash: Trends in Rapid Temperature Changes in a Warming Climate. *Int. J. Climatol.* **2022**, *42*, 4214–4222. [CrossRef]
9. Ault, T.R.; Henebry, G.M.; De Beurs, K.M.; Schwartz, M.D.; Betancourt, J.L.; Moore, D. The False Spring of 2012, Earliest in North American Record. *Eos Trans. AGU* **2013**, *94*, 181–182. [CrossRef]
10. Peterson, T.C.; Hoerling, M.P.; Stott, P.A.; Herring, S.C. Explaining Extreme Events of 2012 from a Climate Perspective. *Bull. Am. Meteorol. Soc.* **2013**, *94*, S1–S74. [CrossRef]
11. Guo, W.; Dai, H.; Qian, J.; Tan, J.; Xu, Z.; Guo, Y. An Assessment of the Relationship between Spring Frost Indicators and Global Crop Yield Losses. *Sci. Total Environ.* **2024**, *954*, 176560. [CrossRef]
12. Liang, T.; Ai, Z.; Zhong, H.; Xiao, M.; Xie, M.; Liang, X.; Li, L. The Impact of Temperature Changes on the Health Vulnerability of Migrant Workers: An Empirical Study Based on the China Family Panel Studies. *Front. Public Health* **2025**, *13*, 1519982. [CrossRef]
13. Armstrong, B.; Gasparrini, A.; Hajat, S. Estimating Mortality Displacement During and After Heat Waves. *Am. J. Epidemiol.* **2014**, *179*, 1405–1406. [CrossRef]
14. Pehlivan, N.; Kang, C.; Lee, W.; Ra, C.K.; Park, C.; Yang, J.; Kwon, D.; Choi, M.; Jang, J.; Ahn, S.; et al. Associations Between Various Types of Mortality and Temperature Variability Distinguishing the Intraday and Interday Effects in South Korea. *Environ. Res.* **2024**, *263*, 120277. [CrossRef]
15. Reuters. Wave of Low Temperature Brings Rare Snowfall to Shanghai. Available online: https://www.reuters.com/business/environment/wave-low-temperature-brings-rare-snowfall-shanghai-2026-01-20/ (accessed on 31 January 2026).
16. Giannakopoulos, K.L.; Furtado, J.C. Examining the Characteristics and Evolution of Wintertime Temperature Whiplash Events in the U.S. Southern Plains. *J. Clim.* **2026**, *39*, 37–49. [CrossRef]

17. Liu, Q.; Fu, C.; Xu, Z.; Ding, A. Global Warming Intensifies Extreme Day-to-Day Temperature Changes in Mid–Low Latitudes. *Nat. Clim. Change* **2026**, *16*, 69–76. [CrossRef]
18. Xu, W.; Ma, S.; Zhu, C. Enhanced Subseasonal Variability of Spring Temperature over Eastern China in 2022: Initial Role of Extremely Heavy Arctic Sea Ice in Previous Winter. *Geophys. Res. Lett.* **2023**, *50*, e2023GL106017. [CrossRef]
19. Yang, Y.; Zhao, R. Urban Population Exposure to Apparent Temperature Whiplash Is Projected to Increase with Global Warming. *Commun. Earth Environ.* **2025**, *7*, 42. [CrossRef]
20. Chan, D.; Wu, Q.; Jiang, G.; Dai, X. Projected Shifts in Köppen Climate Zones over China and Their Temporal Evolution in CMIP5 Multi-Model Simulations. *Adv. Atmos. Sci.* **2016**, *33*, 283–293. [CrossRef]
21. Lee, J.; Son, S.-W.; Cho, H.-O.; Kim, J.; Cha, D.-H.; Gyakum, J.R.; Chen, D. Extratropical Cyclones over East Asia: Climatology, Seasonal Cycle, and Long-Term Trend. *Clim. Dyn.* **2020**, *54*, 1131–1144. [CrossRef]
22. Ying, M.; Yang, Y.; Chen, B.; Zhang, W. Climatic Variation of Tropical Cyclones Affecting China during the Past 50 Years. *Sci. China Earth Sci.* **2011**, *54*, 1226–1237. [CrossRef]
23. Chen, Y.; Liao, Z.; Zhai, P. Coincidence of Increasingly Volatile Winters in China with Arctic Sea-Ice Loss During 1980–2018. *Environ. Res. Lett.* **2019**, *14*, 124076. [CrossRef]
24. Chen, H.; Jiang, J.; Liu, Y. Investigating the December 2023 Warm-to-Cold Weather Whiplash in China Using a Novel Flash-Cold Metric. *Environ. Res. Lett.* **2025**, *20*, 014040. [CrossRef]
25. Li, B.; Chi, Y.; Zhou, H.; Zhang, S.; Lu, Y. The Study of Synergistic Changes in Extreme Cold and Warm Events in the Sanjiang Plain. *Atmosphere* **2024**, *15*, 1092. [CrossRef]
26. Xu, J.; Ma, Z.; Yan, S.; Peng, J. Do ERA5 and ERA5-Land Precipitation Estimates Outperform Satellite-Based Precipitation Products? A Comprehensive Comparison Between State-of-the-Art Model-Based and Satellite-Based Precipitation Products over Mainland China. *J. Hydrol.* **2022**, *605*, 127353. [CrossRef]
27. Yao, N.; Li, Y.; Lei, T.; Peng, L. Drought Evolution, Severity and Trends in Mainland China over 1961–2013. *Sci. Total Environ.* **2018**, *616–617*, 73–89. [CrossRef] [PubMed]
28. Mudelsee, M. Trend Analysis of Climate Time Series: A Review of Methods. *Earth-Sci. Rev.* **2019**, *190*, 310–322. [CrossRef]
29. Yue, S.; Wang, C. The Mann-Kendall Test Modified by Effective Sample Size to Detect Trend in Serially Correlated Hydrological Series. *Water Resour. Manag.* **2004**, *18*, 201–218. [CrossRef]
30. Kelly, K.; Šavrič, B. Area and Volume Computation of Longitude–Latitude Grids and Three-Dimensional Meshes. *Trans. GIS* **2021**, *25*, 6–24. [CrossRef]
31. Zhao, F.F.; Xu, Z.X.; Huang, J.X.; Li, J.Y. Monotonic Trend and Abrupt Changes for Major Climate Variables in the Headwater Catchment of the Yellow River Basin. *Hydrol. Process.* **2008**, *22*, 4587–4599. [CrossRef]
32. Enfield, D.B.; Mestas-Nuñez, A.M.; Trimble, P.J. The Atlantic Multidecadal Oscillation and Its Relation to Rainfall and River Flows in the Continental U.S. *Geophys. Res. Lett.* **2001**, *28*, 2077–2080. [CrossRef]
33. Geng, X.; Zhang, W.; Stuecker, M.F.; Jin, F.-F. Strong Sub-Seasonal Wintertime Cooling over East Asia and Northern Europe Associated with Super El Niño Events. *Sci. Rep.* **2017**, *7*, 3770. [CrossRef] [PubMed]
34. Simolo, C.; Corti, S. Quantifying the Role of Variability in Future Intensification of Heat Extremes. *Nat. Commun.* **2022**, *13*, 7930. [CrossRef] [PubMed]
35. Zhang, W.; Wu, B. The Role of Transient Eddies in the Intraseasonal Reversal of East Asian Winter Air Temperature Anomalies. *Atmos. Res.* **2023**, *289*, 106748. [CrossRef]
36. Ying, K.; Zhao, T.; Quan, X.-W.; Zheng, X.; Frederiksen, C.S. Interannual Variability of Autumn to Spring Seasonal Precipitation in Eastern China. *Clim. Dyn.* **2015**, *45*, 253–271. [CrossRef]
37. Luo, M.; Wang, X.; Dong, N.; Zhang, W.; Li, J.; Wu, S.; Ning, G.; Dai, L.; Liu, Z. Two Different Propagation Patterns of Spatiotemporally Contiguous Heatwaves in China. *npj Clim. Atmos. Sci.* **2022**, *5*, 89. [CrossRef]
38. Stephan, C.C.; Klingaman, N.P.; Vidale, P.L.; Turner, A.G.; Demory, M.-E.; Guo, L. A Comprehensive Analysis of Coherent Rainfall Patterns in China and Potential Drivers. Part II: Intraseasonal Variability. *Clim. Dyn.* **2018**, *51*, 17–33. [CrossRef]
39. Song, L.; Wu, R. Processes for Occurrence of Strong Cold Events over Eastern China. *J. Clim.* **2017**, *30*, 9247–9266. [CrossRef]
40. Wan, N.; Lin, X.; Pielke, R.A. Assessment of Trends in an Integrated Climate Metric—Analysis of 200 Mbar Zonal Wind for the Period 1958–2021. *Theor. Appl. Climatol.* **2022**, *150*, 1217–1230. [CrossRef]
41. Schemm, S.; Papritz, L.; Rivière, G. Storm Track Response to Uniform Global Warming Downstream of an Idealized Sea Surface Temperature Front. *Weather Clim. Dyn.* **2022**, *3*, 601–623. [CrossRef]
42. Abdillah, M.R.; Kanno, Y.; Iwasaki, T.; Matsumoto, J. Cold Surge Pathways in East Asia and Their Tropical Impacts. *J. Clim.* **2021**, *34*, 157–170. [CrossRef]
43. Chen, Y.; Zhai, P. Simultaneous Modulations of Precipitation and Temperature Extremes in Southern Parts of China by the Boreal Summer Intraseasonal Oscillation. *Clim. Dyn.* **2017**, *49*, 3363–3381. [CrossRef]

44. Xu, W.; Li, Y.; Chen, Q.; Zhou, X.; Jiang, X.; Wang, W.; Huyan, L.; Li, X.; Jiang, Y.; Deng, R.; et al. Remote Influence of the Atlantic Multidecadal Oscillation on the Autumn Surface Air Temperature in Southwest China. *Earth Planet. Phys.* **2025**, *9*, 1061–1072. [CrossRef]
45. Guo, R.; Huang, J.; Yu, H.; Zhao, H.; Hu, Z. Decadal Modulation of Temperature Pattern over East Asia by Pacific Decadal Oscillation. *Atmos. Res.* **2024**, *300*, 107248. [CrossRef]
46. Li, S.; Bates, G.T. Influence of the Atlantic Multidecadal Oscillation on the Winter Climate of East China. *Adv. Atmos. Sci.* **2007**, *24*, 126–135. [CrossRef]

Disclaimer/Publisher's Note: The statements, opinions and data contained in all publications are solely those of the individual author(s) and contributor(s) and not of MDPI and/or the editor(s). MDPI and/or the editor(s) disclaim responsibility for any injury to people or property resulting from any ideas, methods, instructions or products referred to in the content.